Scientia Iranica B (2023) 30(1), 64–76

Sharif University of Technology
Scientia Iranica
Transactions B: Mechanical Engineering
http://scientiairanica.sharif.edu

Research Note

Heat transfer enhancement for a cylinder by flexible fins in turbulent flow

I. Zahed[a], Y. Amini[a,*], and E. Izadpanah[a]

Department of Mechanical Engineering, Persian Gulf University, Bushehr, 75169, Iran.

Received 20 October 2021; received in revised form 27 May 2022; accepted 18 October 2022

KEYWORDS
Turbulent flow;
Heat transfer enhancement;
Fluid-structure interaction;
Flexible fins;
Circular cylinder.

Abstract. Heat transfer from circular cylinders in turbulent cross flows plays a significant role in industrial operations. The objective of this paper is to numerically evaluate the heat transfer from a cylinder with a circular cross-section and four flexible fins in turbulent flows. The governing equations of the thermal fluid as well as the equations of the motion of deformable structure of fins were discretized using Finite Element Method (FEM). The designed model was employed to simulate the flow. The obtained results were then validated by comparing the heat transfer rate obtained from the circular cylinder with that from other experimental and numerical studies. In addition, the results from Fluid-Structure Interaction (FSI) were validated with respect to a benchmark example. The flexible fins were glued to the circular cylinder at two different angles of $\theta = 0^\circ$ and $\theta = 45^\circ$. In both cases, the thermal enhancement and flow-induced vibrations of the fins were investigated at different degrees of non-dimensional flexural rigidity. According to the findings in this research, the attached fins at both angles with different flexural rigidity levels significantly affected the Nusselt number. In addition, highly flexible fins cause an increase in Nusselt number by 26%.

© 2023 Sharif University of Technology. All rights reserved.

1. Introduction

Heat exchangers are widely used in cooling and heating systems such as power plants, refrigeration, boiling facilities, chemical plants, electrical apparatuses, and air conditioning systems. In most industrial heat exchangers, convective heat transfer is the dominant process used for heat transfer. In this regard, any enhancement in the convective heat transfer would consequently result in efficiency improvement and size reduction of heat exchangers. Few studies have been conducted on the convective heat transfer from cylinders in the tube-fin heat exchangers and shell and tube [1–4]. A brief review of the related literature indicates that different methods have been proposed for increasing the convective heat transfer rate and they can be mainly divided into two groups of active and passive methods [5]. The convective heat transfer can be enhanced by changes in perturbation and instability in the thermal boundary layer. One of the best methods that ensures such enhancement is Fluid-Structure Interaction (FSI), which occurs when a fluid flow imposes sufficient forces on a deformable structure.

Recently, many researchers have studied the FSI based on the numerical or experimental methods for both laminar and turbulent flows [6–12]. Using a flexible plate as an obstacle to the fluid flow is one of the most common approaches to intensification of heat transfer from the channel walls. Joshi et al. [13]

*. *Corresponding author.*
E-mail address: aminiyasser@pgu.ac.ir (Y. Amini)

doi: 10.24200/sci.2022.59271.6147

considered a flexible fin installed in a channel and used the finite element method to explore its effects on the heat transfer enhancement in the pulsated flows. Further, they studied the effect of Prandtl number, flow frequency, and Young's modulus on the heat transfer rate and found that large, non-uniform, and cyclic heat loads could be dissipated through fins. Ghalambaz et al. [14] numerically examined the free convective heat transfer from a cavity with a flexible fin. They attempted to determine the best length of the fin to enhance the heat transfer and consequently achieved the optimum length. Park et al. [15] measured the heat transfer rate from a flexible floating body using the immersed boundary method. They found that the heat transfer rate could increase up to 7% in the elastic cylinder, compared to the rigid one. Khanafer and Vafai [16] numerically studied the natural convective inside a cavity filled with a porous material. They further investigated the impact of the porous material parameters and deformability of boundaries on the heat transfer performance at different Rayleigh numbers and the wall elasticity values. They concluded that an increase in the Rayleigh number directly affected the heat transfer enhancement. Mehryan et al. [17] examined natural heat transfer in a square cavity with a thin elastic heating plate placed in the middle of the cavity. The vertical and horizontal walls were assumed to be cold and adiabatic, respectively. They also investigated the effects of different inclination angles of this hot plate on the average Nusselt number. Liu [18] analyzed the impact of FSI on both heat and mass transfer in an enclosure. He took into consideration the weakly coupled equations by a staggered-partitioned scheme and second-order accuracy and studied the effects of different parameters on the heat transfer rate.

Amini et al. [19] numerically simulated the effect of fluid structure interaction between the rotating vortex generators and fluid flow on the conjugate heat transfer in a 3D microchannel. They also evaluated different values of the rotation directions, frequencies, and Reynolds numbers and reported an increase in the Nusselt number upon increasing the Reynolds number. Li et al. [20] numerically considered the effect of an elastic angled flap attached to the channel wall on the heat transfer using the COMSOL software. Their obtained results revealed that the Nusselt number increased up to 200% the value in the straight channel. Ali et al. [21] made a comparison of the effects of the flexible flaps with those of the rigid flaps on a channel. They found that the flexible flaps increased the heat transfer up to 134% more than the rigid flaps. In addition, they [22] used several multi-vortex generators in a 2D laminar flow to examine their effects on the heat transfer enhancement. They observed that upon increasing the number of elastic vortex generators, the thermal performance of the channel would also increase. Lee et al. [23,24] put two flags in both symmetrical and asymmetrical configurations and compared their effects on the heat transfer enhancement within the channel. They discovered that the symmetric arrangement increased the heat transfer up to 207% more than the asymmetric one. Chen et al. [25] experimentally placed two flags at different distances to determine their impacts on the thermal performance of the channel walls. They observed that the heat transfer was marginally improved using these reversed flags.

Gallegos et al. [26] experimentally analyzed the thermal characteristics of a rectangular channel with an elastic flag. They studied the effects of the flag and channel shape on the heat transfer enhancement. In the advanced form of obstacles to the fluid flow, an elastic plate was widely studied that was glued to the cylinders in turbulent or laminar flows at a specific distance from the channel wall. According to their observations, the channel width affects the flag dynamics, oscillates in more complex modes, and consequently creates stronger vortices. Creating stronger vortices and delaying turbulence decay consequently enhance the heat transfer in a wider area of the channel. Mohammadshahi et al. [27] studied the heat transfer from an elastic fin glued to a cylinder with a circular cross-section located in a channel based on the numerical methods. They also studied the effects of FSI on the heat transfer enhancement from the channel walls in a turbulent flow. Their results revealed that upon adding an elastic fin connected to the rear of a fixed cylinder, compared to a smooth cylinder, the lift coefficient and mechanical loss increased up to 86% and 31.1%, respectively. In their study, the Nusselt number increased up to 2.3%. With the same geometry, Soti et al. [28] took into account the effect of the Prandtl and Reynolds numbers as well as the elastic properties on the thermal performance enhancement for the channel through finite element method in Newtonian and incompressible laminar flow. They concluded that compared to the rigid cylinder, the flexible plate glued to the rigid cylinder could double the Nusselt number of the channel. Sun et al. [29] numerically studied the forced convection heat transfer from a cylinder with an elastic fin with Prandtl and Reynolds numbers of 0.7 and 200, respectively. In their study, the energy and Navier-Stokes equations were coupled by Euler-Bernoulli beam equation as a model for the flexible fin vibration. They found that the convection heat transfer increased up to 11.07% in this situation. Sun et al. [30] simulated two heated tandem circular cylinders that vibrated in the transverse direction using FSI. Their study provided useful insights into the heat transfer properties of cylindrical structures under fluid-induced vibration. The effects of FSI on the heat transfer rates in the heat exchangers were also notable.

Duan et al. [31] investigated the effects of Planar

Elastic Tube Bundles (PETB) on the heat transfer enhancement in three different flow cases. According to their findings, both pulsing and coupled flows were characterized by higher local Nusselt number than those of the steady flow with maximum increase of 11.4% and 2.8%, respectively. Xie and Zhang [32] used oscillating cylinders as an active technique in order to enhance the convective heat transfer rate. They remarked that this technique helped achieve the maximum improvement of 14.69% in the Nusselt number. Amini and Habibi [33] used multiple elastic vortex generator in a channel in order to intensify the heat transfer rate from the channel. They found that elastic vortex generators could increase the Nusselt number up to 190% compared to the clean channel. Shahrestani et al. [34] numerically evaluated the effects of the deformable walls on the natural convection inside a circular enclosure. According to their observations, Nusselt number increased more than five times upon increasing the Ra number. Zhong et al. [35] examined the effects of the inverted flags attached to the walls of a channel on the heat transfer rate and concluded that these types of flags could significantly increase the Nusselt number of heat sinks. Hakim et al. [36] suggested a numerical method for FSI problem under the effect of an elastic flow regulator. In their study, both FSI and heat transfer rate significantly increased by the external vibration and elasticity of the flow regulator. Mehryan et al. [37] considered an elastic splitter plate within a square cavity with various inclined-angle and different positions to examine its effect on the natural convection of a cavity. Dey [38] studied the dual splitter plates placed on the top and bottom of a square cylinder with different lengths to assess their effect on the heat transfer of a cylinder. Consequently, heat transfer was enhanced up to 40%, compared to that of the bare cylinder.

The current study aimed to evaluate the effects of elastic fins on the convective heat transfer rate from a cylinder with a circular cross-section in a turbulent flow. To this end, four elastic fins were taken into consideration that were glued to a cylinder. In addition, the constant temperature boundary conditions for cylinder and flexible fins were taken into consideration. Two different configurations of fins were investigated in an extensive range of non-dimensional flexural rigidities.

2. Governing equations

In the FSI problem, the structural governing equation is coupled to the governing equation of the fluid flow. Physically, the fluid flow imposes hydrodynamic forces on the structure that causes deformation, hence movement of the fluid flow boundaries. Monolithic and partitioned approaches are the main methods that are used for simulating the FSI problems. In the monolithic approach, the governing equations of both structure and fluid flow are solved by a single solver. In the other approach used in this study, two separated solvers are utilized to solve the governing equations of the fluid and structure. Here, the fluid flow is considered Newtonian, incompressible, and turbulent; therefore, the governing equations can be written as follows:

$$\frac{\partial v_i}{\partial x_i} = 0, \tag{1}$$

$$\rho\left(\frac{\partial v_i}{\partial t} + v_j\frac{\partial v_i}{\partial x_j}\right) = -\frac{\partial P}{\partial x_i} + \frac{\partial}{\partial x_j}\left((\mu+\mu_t)\frac{\partial v_i}{\partial x_j}\right), \tag{2}$$

where v is the velocity in the ith direction. Given that Shear Stress Transport (SST) $k-\omega$ model [39] accurately predicts the adverse gradient and separated flows, it is employed to capture the turbulent nature of the fluid flow. The specific dissipation rate (ω) and turbulence kinetic energy (k) equations are as follows:

$$\frac{\partial k}{\partial t} + v_j\frac{\partial k}{\partial x_j} = P_k - \beta^* k\omega + \frac{\partial}{\partial x_j}\left[\left(\frac{\mu+\sigma_k\mu_t}{\rho}\right)\frac{\partial k}{\partial x_j}\right], \tag{3}$$

$$\frac{\partial \omega}{\partial t} + v_j\frac{\partial \omega}{\partial x_j} = aS^2 - \beta\omega^2 + \frac{\partial}{\partial x_j}\left[\left(\frac{\mu+\sigma_\omega\mu_t}{\rho}\right)\frac{\partial \omega}{\partial x_j}\right] + 2(1-F_1)\frac{\sigma_{\omega_2}}{\omega}\frac{\partial k}{\partial x_j}\frac{\partial \omega}{\partial x_j}. \tag{4}$$

P_k, β^*, a, β, S, σ_ω, $\sigma_{\omega 2}$ were expressed in [39]. In addition, μ_t is the eddy viscosity that can be defined as:

$$\mu_t = \rho\frac{k}{\omega}. \tag{5}$$

Moreover, the energy equation is defined as:

$$\frac{\partial T}{\partial t} + v_j\frac{\partial T}{\partial x_j} = \frac{\partial}{\partial x_j}\left((\alpha+\alpha_t)\frac{\partial T}{\partial x_j}\right), \tag{6}$$

where T, α, and α_t are the temperature, molecular diffusivity, and turbulent thermal diffusivity, respectively. In the following, the equations of the motion of an isotropic and elastic material are given:

$$\frac{\partial \sigma_{ij}}{\partial x_j} + \rho_s b_i = \rho_s\frac{\partial u_i}{\partial t}, \tag{7}$$

$$\sigma_{ij} = \frac{E}{1+v}\left(\varepsilon_{ij} + \frac{v}{1-2v}\varepsilon_{kk}\delta_{ij}\right), \tag{8}$$

$$\varepsilon_{ij} = \frac{1}{2}\left(\frac{\partial u_i}{\partial x_j} + \frac{\partial u_j}{\partial x_i} + \frac{\partial u_k}{\partial x_i}\frac{\partial u_k}{\partial x_j}\right), \tag{9}$$

where b is the force per volume, σ_{ij} the stress tensor, v the Poisson's ratio, E the Young's modulus, and δ_{ij} the Kronecker delta. Eqs. (7) and (8) are called the equilibrium and constitutive equations, respectively.

The nondimensional flexural rigidity of fins (EI^*) is defined as:

$$EI^* = \frac{EI}{\rho_f U_{in}^2 D^4}, \tag{10}$$

where the second moment of area is represented by I. The Strouhal number (St) is defined as follows:

$$St = \frac{fD}{U}, \tag{11}$$

where f is the frequency obtained from the time changes of the lift coefficient. Further, the local Nusselt number is calculated via Eq. (12):

$$Nu_{(\theta.t)} = \frac{D}{(T_W - T_\infty)} \frac{\partial T}{\partial n}|_{(\theta.t)}, \tag{12}$$

where n, T_w, and T_∞ are the unit normal vector on the surface of cylinder and fins, temperature of the wall, and inlet temperature, respectively. Average Nusselt number is achieved by integrating its local value over the one-time period of its fluctuations.

3. Problem description

Figure 1 shows the computational domain for the cylinder of D in diameter and their attached elastic fins. The computational domain is rectangle in shape with the dimensions of $195D \times 120D$, and the cylinder is placed at distances of $45D$ and $150D$ from the inlet and outlet boundaries, respectively. In addition, the upper and lower boundaries have equal distances from the cylinder. The length and thickness of the flexible fins are taken to be $1.5D$ and $0.1D$, respectively. Moreover, two different values of the fins angle were obtained as $\theta = 0°$ and $\theta = 45°$.

The inlet velocity and temperature are equal to 1 m/s and 300 K, respectively. Moreover, at lateral boundaries, the slip condition is applied where the normal velocity component is set to zero. On the cylinder surface and plate walls, two conditions of no-slip boundary and constant temperature of 400 K were applied.

The present research used the second-order upwind scheme for discretization of the convection terms in energy and momentum equations and the COUPLE scheme for solving the pressure-velocity coupled problem. The values of the specific heat, fluid density, thermal conductivity, and dynamic viscosity were obtained as $C_p = 3186 \frac{j}{kg.k}$, $\rho_f = 1000 \frac{kg}{m^3}$, $k = 0.4 \frac{w}{m.k}$, and $\mu = 0.001 \frac{kg}{m.s}$, respectively. In this regard, the Prandtl and Reynolds numbers were equal to 7.92 and 10^5, respectively. In addition, the values of solid density and Poisson's ratio were equal to $\rho_s = 10000 \frac{kg}{m^3}$, and $v = 0.4$, respectively. Moreover, the time step was assumed to be 0.005 s. In the current study, an extensive range of Young's moduli were employed to investigate their effects on the heat transfer rate.

4. Validation

The values of the Nusselt number, drag and lift coefficients, and Strouhal number of a fixed cylinder with a circular cross-section for both laminar flow at Re = 150 and Pr = 0.7 and turbulent flows at Re = 3900 and Pr = 0.7 were compared with those already obtained in the literature, as shown in Table 1. The Nusselt number values were compared by experimental correlations derived from Eq. (13) [40] and Eq. (14) [41]:

$$\overline{Nu} = 0.3 + \frac{0.62\ Re^{1/2}\ \mathrm{Pr}^{1/3}}{[1+(0.4/Pr)^{2/3}]^{1/4}} \left[1+\left(\frac{Re}{282000}\right)^{5/8}\right]^{4/5}, \tag{13}$$

$$\overline{Nu} = 0.638\ Re^{0.466}\ Pr^{1/3}. \tag{14}$$

Table 1 confirms excellent agreement between the previous results and those obtained in this study. Figure 2 compares the present time-averaged local

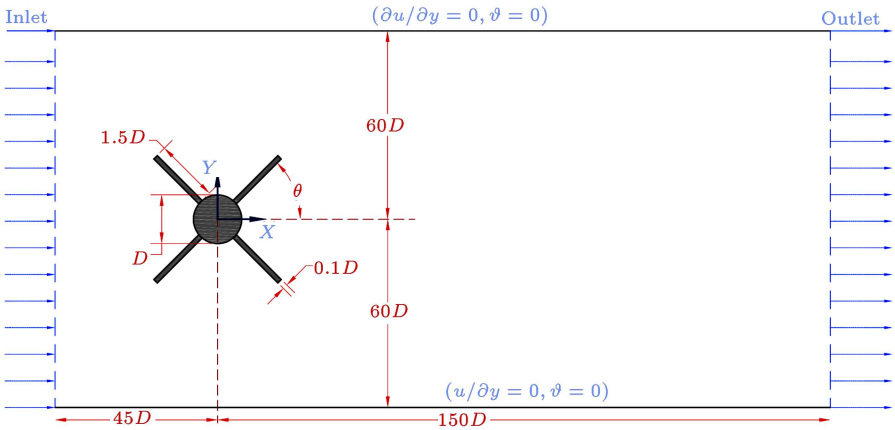

Figure 1. Schematics diagram of computational domain

Table 1. Nusselt number, drag and lift coefficients, and Strouhal number of a fixed cylinder

Re			Cl	St	
Re = 150 Pr = 0.7	Present study	1.343	± 0.498	0.179	6.429
	Izadpanah at el. [3]	1.355	± 0.534	0.187	6.395
	Mahír and Altaç [44]				6.383
	Eq. (13) [40] (**Expt.**) Eq. (14) [41] (**Expt.**)				6.26 6.26
Re = 3900 Pr = 0.7	Present study	1.027	± 0.429	0.203	31.44
	Kravchenkoand and Moin [45]	1.04	—	0.21	
	Eq. (13) [40] (**Expt.**)				32.11

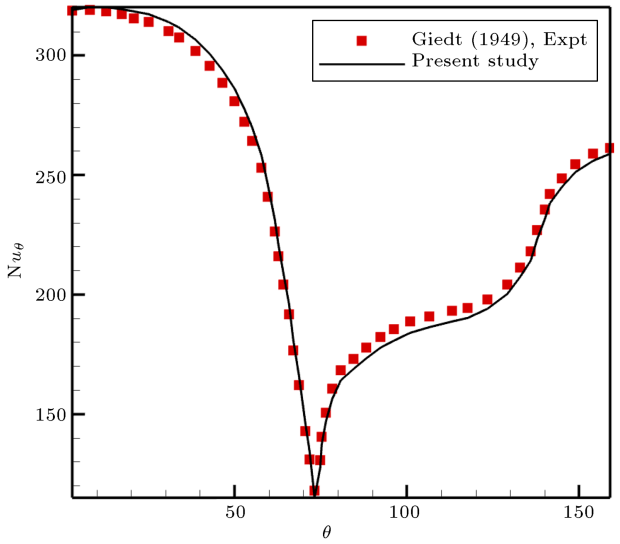

Figure 2. Local Nusselt number (time-averaged) for a circular cylinder at $Re = 101,300$ and $Pr = 0.7$

Nusselt number on the circular cylinder wall with those reported by Giedt [42] at Reynolds number of 101300 and Pr = 0.7. As observed, the Nu number obtained in this study is in good agreement with those obtained from the literature.

Turek and Hron's FSI problem [43] was utilized as the second validation test case. In this test case, a stationary cylinder with an elastic beam located at the center of a channel was investigated in a laminar flow with considered dimensionless Young's modulus of 1.4e3, Reynolds number of 100, and density ratio of 10. In Figure 3, the current calculation for the transverse deflection of the tip point flexible beam was compared with that given by Turek and Hron's FSI problem [43]. As observed, there is good agreement between the obtained results and those from [43].

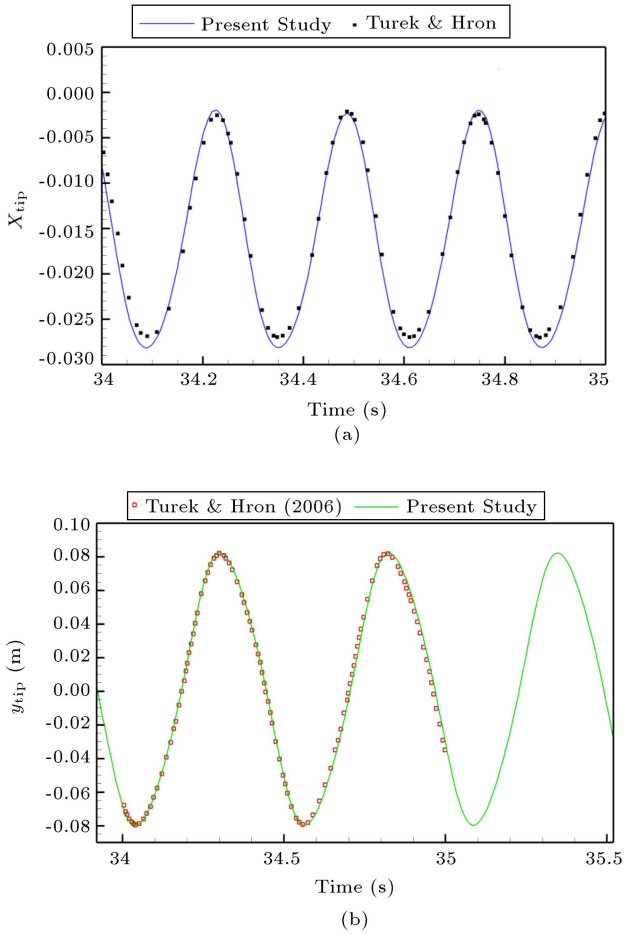

Figure 3. Displacement of end point of elastic plate in (a) inline and (b) transverse directions

5. Grid independence study

In order to investigate independency of the results from a number of grid points, three grids with different densities for the first configuration ($\theta = 0°$) at $EI^* = 6.67$ were taken into account. The number of elements in the fine, medium, and coarse meshes was 212000, 121400, and 76300, respectively. Figure 4 shows the fully-structured and high-quality fine mesh used for simulations in this study. This mesh is refined close to

Table 2. Deformation of back and top fins $\theta = 0^\circ$ at $EI* = 6.667$.

	Nu_{ave}	C_d	Fin#1	Fin#2		Fin#3		Fin#4		
Coarse	517	10.87	-0.04	0.018	0.57	-0.10	0.08	0.02	0.54	0.14
Medium	495	10.67	-0.04	0.006	0.59	-0.11	0.07	0.02	0.56	0.15
Fine	492	10.62	-0.03	0.005	0.58	-0.11	0.06	0.02	0.56	0.15

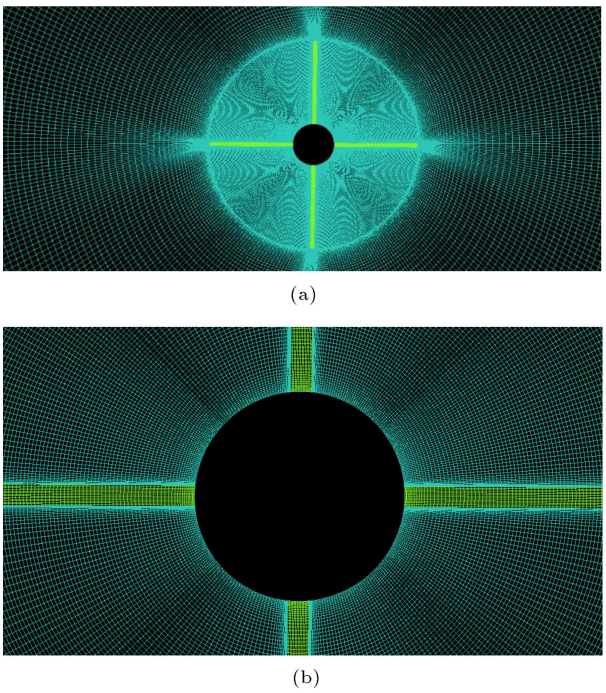

Figure 4. Close-up view of generated mesh for (a) part of the computational domain and (b) around the cylinder and fins

the solid walls to guarantee that the $y^+ < 5$ criterion is achieved for obtaining accurate results from the $k - \omega$ SST model.

Table 2 makes a comparison among the average Nusselt numbers, lift and drag coefficients, and horizontal and vertical components of the tip displacement for these meshes at $EI^* = 6.67$. Apparently, the differences between the data of the medium grid and those of fine mesh are insignificant. Therefore, the number of elements of the medium mesh is adequate enough to accurately simulate the FSI problem.

6. Results and discussion

Figure 5 shows the flow streamlines for $\theta = 0^\circ$ (first configuration) versus EI^*. The time difference between two consecutive contours at each value of EI^* is $\Gamma/2$, where Γ stands for the period of vibration of the fin tip point. It was also observed that a huge vortex was generated behind the cylinder which was related to the separation of flow from upper and lower tips of the fins. In addition, small vortices generated between the fins impose forces on the fins, thus causing large displacement. Upon decreasing EI^*, deformation of the fins will be intensified, thus affecting the vortex formation and shedding pattern. Another important point is the different deformations of the cylinder fins. For low values of EI^*, the front fin is considerably deformed, thus affecting the flow pattern through the cylinder. As a result, the degree of deformation of the other three fins varies. However, at high values of EI^*, deformation of the upper and lower fins is more significant than that of the front and rear fins.

Figure 6 shows the streamlines of the second configuration ($\theta = 45^\circ$) for different values of EI^*. The time difference between the two consecutive contours is $\Gamma/2$. In this case, due to the position of the fins, the flow separation occurs earlier than the case of $\theta = 0^\circ$, thus affecting the imposed forces and heat transfer. As observed, big vortices are created between the fins. These vortices are combined that create a large vortex behind the cylinder. The results showed that for $\theta = 45^\circ$, the displacement of the two rear fins was more considerable than that of the front fins. Similar to the previous case, it was observed that upon decreasing EI^* in this case, the deformation of fins was intensified, especially for the two fins at behind the cylinder.

Figure 7 presents the temperature contours for the first configurations ($\theta = 0^\circ$). The time difference between the two consecutive contours is $\Gamma/8$. In these figures, the effects of vortices on the temperature field are shown. According to the results, the temperature distribution along the cylinder and fins was different for any EI^* mainly due to the variations in the deformation of fins and flow pattern for different values of EI^*. With the reduction of EI^*, the deformation of fins is intensified and consequently, the thermal boundary layer frequently varies, hence a rise in the heat transfer variation.

Figure 8 presents the temperature contours for the second configuration. The time difference between two consecutive contours is $\Gamma/8$. This figure also shows the effects of vortices on the temperature field. As opposed to the first configuration ($\theta = 0^\circ$), the high-

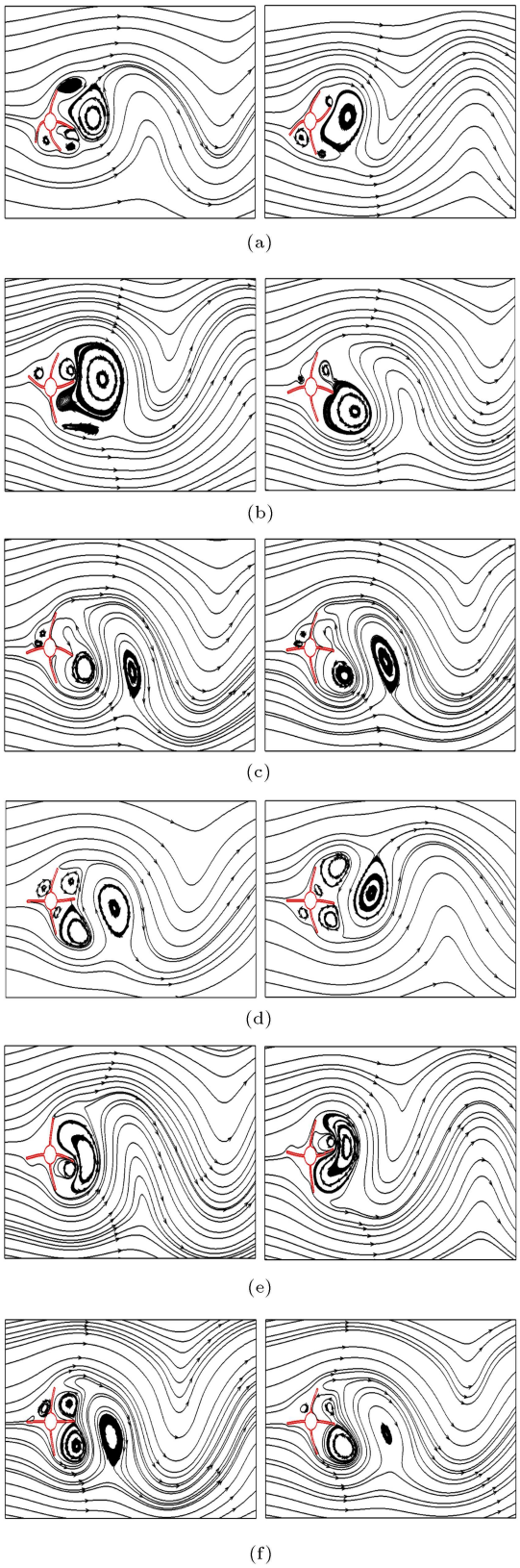

Figure 5. Streamlines for the first configuration ($\theta = 0°$) at the times of t_0 and $t_0 + \frac{\Gamma}{2}$ for (a) $EI^* = 5$, (b) $EI^* = 6.68$, (c) $EI^* = 8.33$, (d) $EI^* = 10$, (e) $EI^* = 16.67$, and (f) $EI^* = 20$.

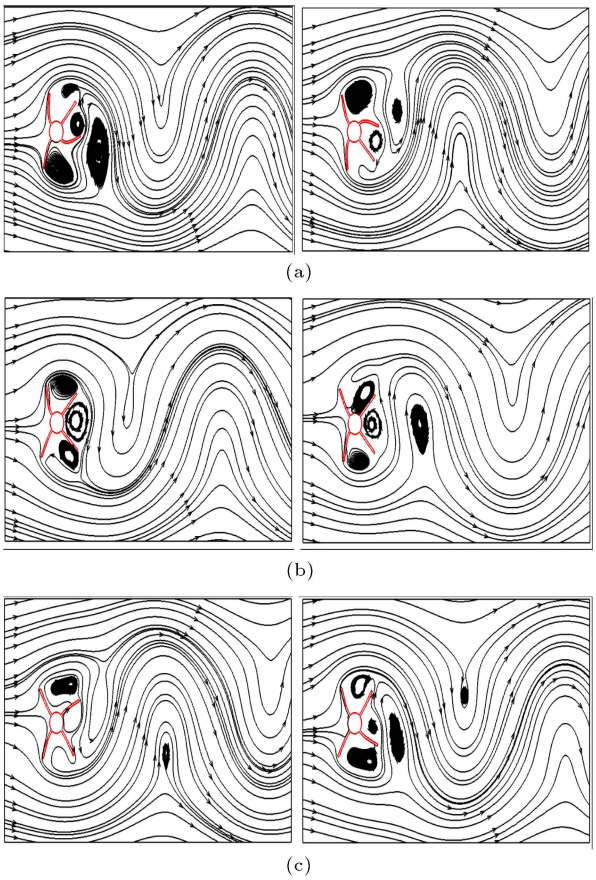

Figure 6. Streamlines for the second configuration ($\theta = 45°$) at the times of t_0 and $t_0 + \frac{\Gamma}{2}$ for (a) $EI^* = 8.33$, (b) $EI^* = 13.33$, and (c) $EI^* = 20$

temperature region ahead of the cylinder vanishes, leading to the formation of a high-temperature region in the back of the cylinder. This high temperature zone periodically is affected by the vortex shedding from the fins.

Figure 9 shows the time history of the average Nusselt number of cylinder-fins assembly (Nu_{av}) at different values of flexural rigidity. As observed in this figure, Nu_{av} at each time for $EI^* = 3.33$ and 5 is significantly larger than other values of EI^*. On the contrary, the Nusselt number has the lowest value for $EI^* = 6.67$ at each time.

Figure 10 shows the time histories of average Nusselt number for the second configuration ($\theta = 45°$) according to which the average Nusselt number versus time variations is not harmonic, hence completely disordered mainly due to the erratic movement of the fins. The average Nusselt number has the largest value in $EI^* = 20$ at all times.

Figure 11 makes a comparison between the tip displacements of fins numbers #3 and #4 in both configurations ($\theta = 0°$ and $\theta = 45°$). In both configurations, the tip displacement approaches zero as EI^* value increases. Moreover, for all values of flexural

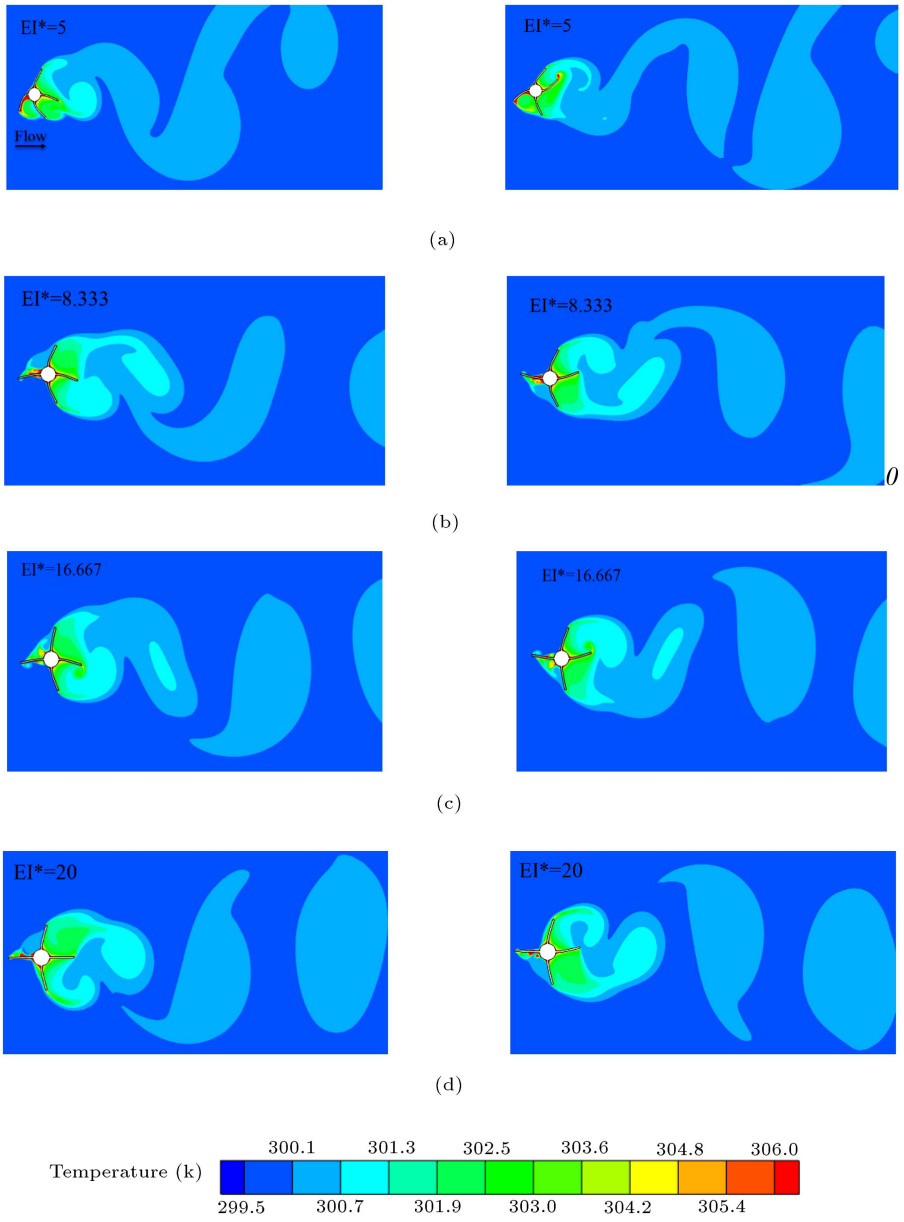

Figure 7. Temperature contours for the first configuration ($\theta = 0^\circ$) at the times of t_0 and $t_0 + \frac{\Gamma}{2}$ for (a) $EI^* = 5$, (b) $EI^* = 8.33$, (c) $EI^* = 16.67$, and (d) $EI^* = 20$.

rigidity, the horizontal component of displacement of fin#3 at $\theta = 45^\circ$ is greater than $\theta = 0^\circ$. However, the x-component of displacement of fin #4 at $\theta = 45^\circ$ is smaller than $\theta = 0^\circ$. The displacement x in both configurations approaches each other at high values of EI^*. For fin #3, the y-displacement of $\theta = 0^\circ$ is greater than $\theta = 45^\circ$ at small values of EI^*.

Figure 12 shows the variation of time-averaged Nusselt number of cylinder and its fins ($\overline{Nu}$) with EI^* for both configurations. For the first configuration ($\theta = 0^\circ$), using fins with high flexibility ($EI^* < 5$) leads to a significant increase in the Nusselt number. In this situation, compared to the rigid fins, the Nusselt number increased up to 26%. For $5 < EI^* < 6$, the Nusselt number decreased by increasing the flexural rigidity. However, the value of the Nusselt number in highly flexible fins is still larger than that in the rigid fins. For the flexural rigidity values between 6 and 13, the value of the Nusselt number is smaller than that in the rigid fins. Finally, for $EI^* > 13$, the flexibility of fins considerably decreased, thus exhibiting the same behavior as that of rigid fins. Therefore, the value of the Nusselt number for $EI^* > 13$ is approximately constant. In the second configuration ($\theta = 45^\circ$), for $11.5 < EI^* < 15$, the Nusselt number is smaller than that in the rigid fins. For $EI^* > 15$, the Nusselt number is approximately equal to its value in the rigid fins. For $EI^* < 11.5$, the Nusselt number is

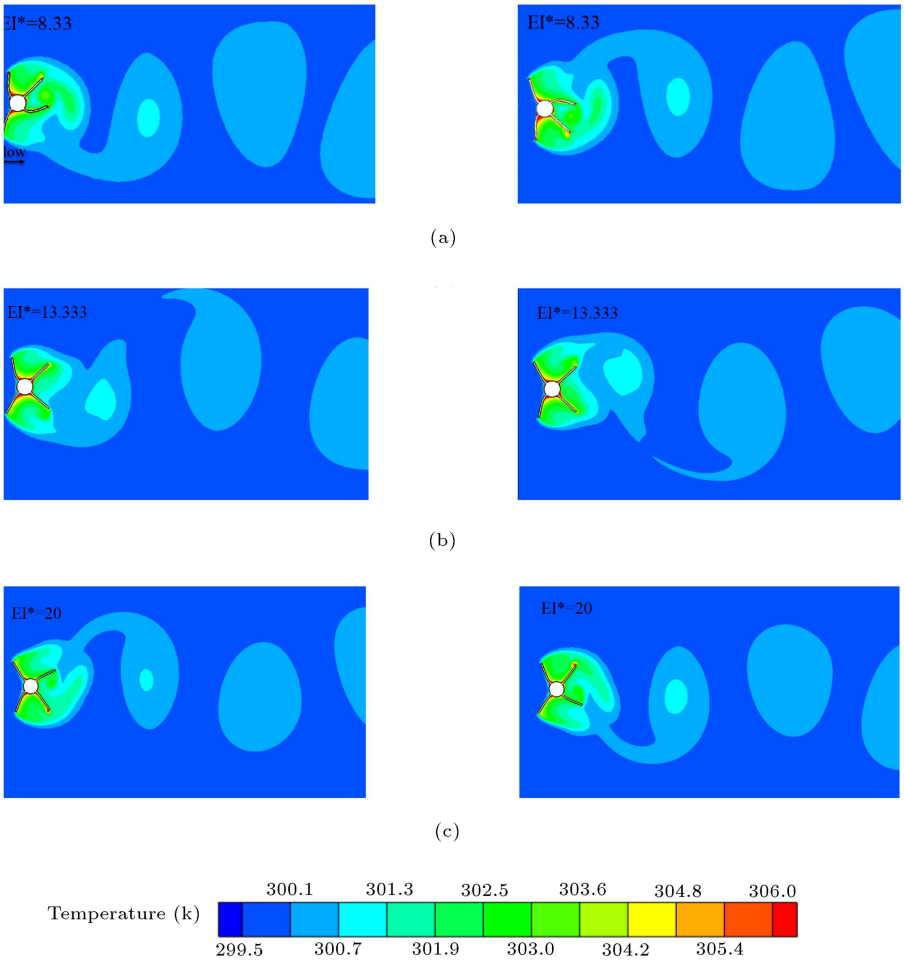

Figure 8. Temperature contours for the first configuration ($\theta = 45°$) at the times of t_0 and $t_0 + \frac{\Gamma}{2}$ for (a) $EI^* = 8.33$, (b) $EI^* = 13.33$, and (c) $EI^* = 20$.

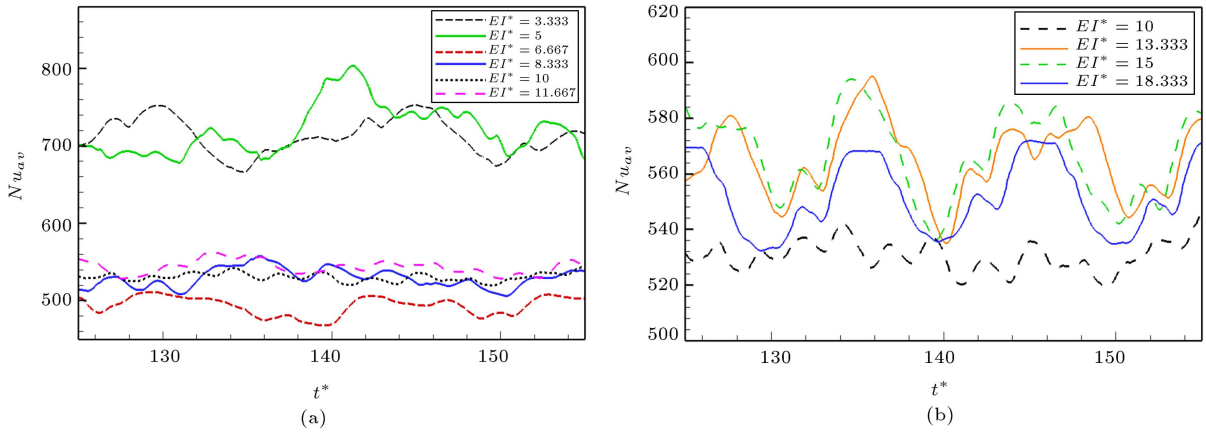

Figure 9. The averaged Nusselt number for $\theta = 0°$ at (a) $EI^* = 3.33, 5, 6.67, 8.33, 10, 11.67$ and (b) $EI^* = 10, 13.33, 15, 18.33$.

a bit larger than that in the rigid fins. It can be concluded that in this configuration, except for the range of $11.5 < EI^* < 15$, the value of the Nusselt number is approximately equal to that of the rigid fins.

Conclusion

The present research aimed to numerically study the effects of four elastic fins on the heat transfer characteristics of a cylinder in turbulent flow. In this

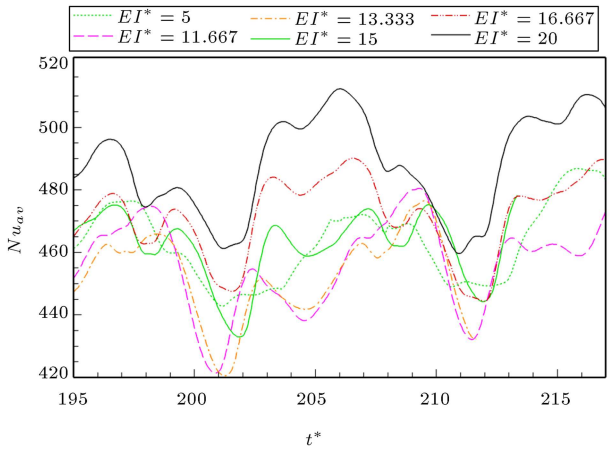

Figure 10. The time histories of averaged Nusselt number for $\theta = 45°$ at various flexural rigidity.

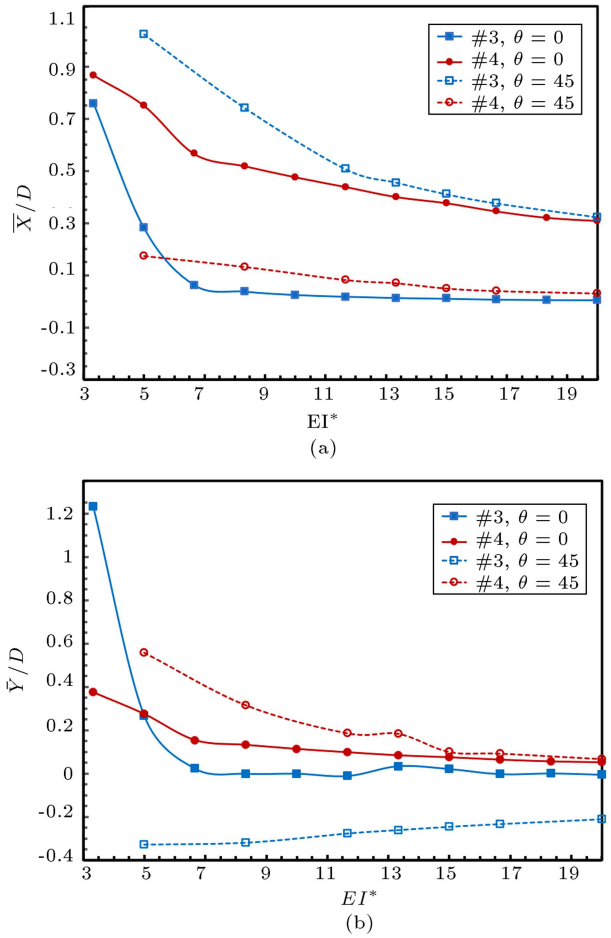

Figure 11. The displacements of fins' tips of 3 and 4 in (a) in-line and (b) transverse directions for $\theta = 0°$ and $\theta = 45°$.

regard, the turbulent flow was simulated through the $k - w$-SST model. It was found that in the first configuration ($\theta = 0°$), the flexibility of fins greatly affected the Nusselt number. In this configuration, for a high-flexibility region ($EI^* < 6$), the Nusselt number increased up to 26%, compared to the rigid

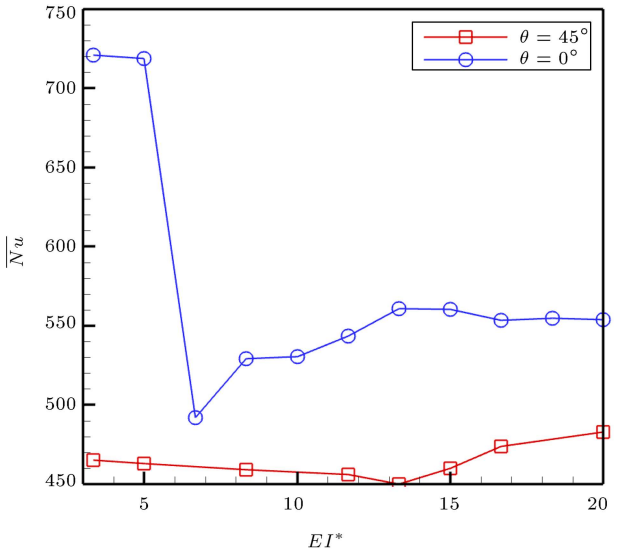

Figure 12. Time-averaged Nusselt number versus various dimensionless flexural rigidity for $\theta = 0°$ and $\theta = 45°$

fins. For the flexural rigidity between 6 and 13, the flexibility had negative effects on the Nusselt number and reduced the Nusselt number, compared to the rigid fins. In the second configuration ($\theta = 45°$), the flexibility of the fins had negligible effect on the Nusselt number. However, for $EI^* < 13$, the Nusselt number increased upon increasing the flexibility of fins.

Availability of data and material

The data that support the findings of this study are available upon reasonable request.

Nomenclature

Alphabetical symbols

D	Diameter of cylinder
L	Length of fins
P	Pressure
E	Young's modulus
I	Second moment of area
T	Fluid Temperature
k	Thermal conductivity
t	Time
C_p	Specific heat
U	Velocity

Latina symbols

θ	Degree between fin and x-axis
μ	Kinematic viscosity
μ_t	Eddy viscosity

k	Turbulence kinetic energy
ω	Specific dissipation rate
α	Thermal diffusivity
ρ	Density
ϑ	Passion's ratio

Dimensionless number

EI^*	Non-dimensional flexural rigidity
$t*$	Non-dimensional time
Pr	Prandtl number
Nu	Nusselt number
$\overline{Nu}$	Average Nusselt number
St	Strouhal number
Re	Reynolds number

Subscripts

f	Fluid
s	Structure
w	Wall
av	Average
In	inlet
out	Outlet

References

1. Izadpanah, E., Ashouri, A., Liravi, M., et al. "Effect of vortex-induced vibration of finned cylinders on heat transfer enhancement", *Physics of Fluids*, **31**(7), p. 073604 (2019).
2. Hadad, Y. and Jafarpur, K. "Laminar forced convection heat transfer from isothermal cylinders with active ends and different aspect ratios in axial air flows", *Heat and Mass Transfer*, **47**(1), pp. 59–68 (2011).
3. Izadpanah, E., Amini, Y., and Ashouri, A. "A comprehensive investigation of vortex induced vibration effects on the heat transfer from a circular cylinder", *International Journal of Thermal Sciences*, **125**, pp. 405–418 (2018).
4. Liu, J.-C., Wei, X.-T., Zhou, Z.-Y., and Wei, Z.-W. "Numerical analysis on interactions between fluid flow and structure deformation in plate-fin heat exchanger by Galerkin method", *Heat and Mass Transfer*, **54**(9), pp. 2835–2844 (2018).
5. Bergles, A.E. "Techniques to augment heat transfer", *Handbook of Heat Transfer (A 74-17085 05-33)*, New York, McGraw-Hill Book Co., p. 10–1 (1973).
6. Amini, Y., Emdad, H., and Farid, M. "A new model to solve fluid-hypo-elastic solid interaction using the smoothed particle hydrodynamics (SPH) method", *European Journal of Mechanics–B/Fluids*, **30**(2), p. 184–194 (2011).
7. Amini, Y., Emdad, H., and Farid, M. "An accurate model for numerical prediction of piezoelectric energy harvesting from fluid structure interaction problems", *Smart Materials and Structures*, **23**(9), p. 095034 (2014).
8. Bazilevs, Y., Korobenko, A., Deng, X., and Yan, J. "Novel structural modeling and mesh moving techniques for advanced fluid-structure interaction simulation of wind turbines", *International Journal for Numerical Methods in Engineering*, **102**(3–4), pp. 766–783 (2015).
9. Amini, Y., Emdad, H., and Farid, M. "Fluid-structure interaction analysis of a piezoelectric flexible plate in a cavity filled with fluid", *Scientia Iranica, Transactions B, Mechanical Engineering*, **23**(2), p. 559 (2016).
10. Müller, A., Favrel, A., Landry, C., et al. "Fluid-structure interaction mechanisms leading to dangerous power swings in Francis turbines at full load", *Journal of Fluids and Structures*, **69**, pp. 56–71 (2017).
11. Amini, Y., Emdad, H., and Farid, M. "Piezoelectric energy harvesting from vertical piezoelectric beams in the horizontal fluid flows", *Scientia Iranica*, **24**(5), pp. 2396–2405 (2017).
12. Amini, Y. and Zahed, I. "Flow-induced vibration of two tandemly arranged circular cylinders with attached splitter plates", *Ocean Engineering*, **237** p. 109604 (2021).
13. Joshi, R.U., Soti, A.K., and Bhardwaj, R. "Numerical study of heat transfer enhancement by deformable twin plates in laminar heated channel flow", *Computational Thermal Sciences: An International Journal*, **7**(5–6), pp. 467–476 (2015).
14. Ghalambaz, M., Jamesahar, E., Ismael, M.A., et al. "Fluid-structure interaction study of natural convection heat transfer over a flexible oscillating fin in a square cavity", *International Journal of Thermal Sciences*, **111**, pp. 256–273 (2017).
15. Park, S.G., Chang, C.B., Kim, B., et al. "Simulation of fluid-flexible body interaction with heat transfer", *International Journal of Heat and Mass Transfer*, **110**, pp. 20–33 (2017).
16. Khanafer, K. and Vafai, K. "Effect of a circular cylinder and flexible wall on natural convective heat transfer characteristics in a cavity filled with a porous medium", *Applied Thermal Engineering*, **181**, p. 115989 (2020).
17. Mehryan, S.A.M., Alsabery, A., Modir, A., et al. "Fluid-structure interaction of a hot flexible thin plate inside an enclosure", *International Journal of Thermal Sciences*, **153**, p. 106340 (2020).
18. Liu, B. "A Nitsche stabilized finite element method: Application for heat and mass transfer and fluid-structure interaction", *Computer Methods in Applied Mechanics and Engineering*, **386**, p. 114101 (2021).
19. Amini, Y., Akhavan, S., and Izadpanah, E. "A numerical investigation on the heat transfer characteristics of nanofluid flow in a three-dimensional microchannel with harmonic rotating vortex generators", *Journal of Thermal Analysis and Calorimetry*, **139**(1), pp. 755–764 (2020).

20. Li, Z., Xu, X., Li, K., et al. "A flapping vortex generator for heat transfer enhancement in a rectangular airside fin", *International Journal of Heat and Mass Transfer*, **118**, pp. 1340–1356 (2018).
21. Ali, S., Habchi, C., Menanteau, S., et al. "Heat transfer and mixing enhancement by free elastic flaps oscillation", *International Journal of Heat and Mass Transfer*, **85**, pp. 250–264 (2015).
22. Ali, S., Menanteau, S., Habchi, C., et al. "Heat transfer and mixing enhancement by using multiple freely oscillating flexible vortex generators", *Applied Thermal Engineering*, **105**, pp. 276–289 (2016).
23. Lee, J.B., Park, S.G., Kim, B., et al. "Heat transfer enhancement by flexible flags clamped vertically in a Poiseuille channel flow", *International Journal of Heat and Mass Transfer*, **107**, pp. 391–402 (2017).
24. Lee, J.B., Park, S.G., and Sung, H.J. "Heat transfer enhancement by asymmetrically clamped flexible flags in a channel flow", *International Journal of Heat and Mass Transfer*, **116** pp. 1003–1015 (2018).
25. Chen, Y., Yu, Y., Zhou, W., et al. "Heat transfer enhancement of turbulent channel flow using tandem self-oscillating inverted flags", *Physics of Fluids*, **30**(7), p. 075108 (2018).
26. Gallegos, R.K.B. and Sharma, R.N. "Heat transfer performance of flag vortex generators in rectangular channels", *International Journal of Thermal Sciences*, **137**, pp. 26–44 (2019).
27. Mohammadshahi, S., Nili-Ahmadabadi, M., Samsam-Khayani, H., et al. "Numerical study of a vortex-induced vibration technique for passive heat transfer enhancement in internal turbulent flow", *European Journal of Mechanics–B/Fluids*, **72**, pp. 103–113 (2018).
28. Soti, A.K., Bhardwaj, R., and Sheridan, J. "Flow-induced deformation of a flexible thin structure as manifestation of heat transfer enhancement", *International Journal of Heat and Mass Transfer*, **84**, pp. 1070–1081 (2015).
29. Sun, X., Ye, Z., Li, J., et al. "Forced convection heat transfer from a circular cylinder with a flexible fin", *International Journal of Heat and Mass Transfer*, **128**, pp. 319–334 (2019).
30. Sun, X., Li, S., Lin, G.-G., et al. "Effects of flow-induced vibration on forced convection heat transfer from two tandem circular cylinders in laminar flow", *International Journal of Mechanical Sciences*, **195**, p. 106238 (2021).
31. Duan, D., Cheng, Y., Ge, M., et al. "Experimental and numerical study on heat transfer enhancement by Flow-induced vibration in pulsating flow", *Applied Thermal Engineering*, **207**, p. 118171 (2022).
32. Xie, P. and Zhang, X. "Study of laminar convection heat transfer in single-side-heating small-scale cooling channel with vibration cylinder", *International Communications in Heat and Mass Transfer*, **120**, p. 105030 (2021).
33. Amini, Y. and Habibi, S.E. "Effects of multiple flexible vortex generators on the hydrothermal characteristics of a rectangular channel", *International Journal of Thermal Sciences*, **175**, p. 107454 (2022).
34. Shahrestani, A.B., Alshuraiaan, B., and Izadi, M. "Combined natural convection-FSI inside a circular enclosure divided by a movable barrier", *International Communications in Heat and Mass Transfer*, **126**, p. 105426 (2021).
35. Zhong, X., Fu, S., Chan, K., Wang, et al. "Experimental and numerical study of heat transfer performance of a channel flow with an inverted flag", *International Journal of Heat and Mass Transfer*, **193**, p. 122969 (2022).
36. Hakim, M.A., Ahad, A.I., Karim, A.U., et al. "Fluid structure interaction and heat transfer enhancement with dynamic flexible flow modulator", *International Communications in Heat and Mass Transfer*, **134**, p. 105983 (2022).
37. Mehryan, S., Alsabery, A., Modir, A., et al. "Fluid-structure interaction of a hot flexible thin plate inside an enclosure", *International Journal of Thermal Sciences*, **153**, p. 106340 (2020).
38. Dey, P. "Fluid flow and heat transfer around square cylinder with dual splitter plates arranged at novel positions", *Proceedings of the Institution of Mechanical Engineers, Part C: Journal of Mechanical Engineering Science*, **236**(9), pp. 5060–5077 (2022).
39. Menter, F.R. "Two-equation eddy-viscosity turbulence models for engineering applications", *AIAA Journal*, **32**(8), pp. 1598–1605 (1994).
40. Churchill, S. and Bernstein, M. "A correlating equation for forced convection from gases and liquids to a circular cylinder in cross flow", *Journal of Heat Transfer*, **99**(2), pp. 300–306 (1977).
41. Knudsen, J.G., Katz, D.L., and Street, R.E. "Fluid dynamics and heat transfer", *Physics Today*, **12**, p. 40 (1959).
42. Giedt, W. "Investigation of variation of point unit heat transfer coefficient around a cylinder normal to an air stream", *Trans. ASME*, **71**, pp. 375–381 (1949).
43. Turek, S. and Hron, J. *Proposal for Numerical Benchmarking of Fluid-Structure Interaction between an Elastic Object and Laminar Incompressible Flow, Fluid-Structure Interaction*, (2006), Springer, p. 371–385.
44. Mahir, N. and Altaç, Z. "Numerical investigation of convective heat transfer in unsteady flow past two cylinders in tandem arrangements", *International Journal of Heat and Fluid Flow*, **29**(5), p. 1309–1318 (2008).
45. Kravchenko, A.G. and Moin, P. "Numerical studies of flow over a circular cylinder at Re D= 3900", *Physics of Fluids*, **12**(2), pp. 403–417 (2000).

Biography

Iman Zahed received his MSc under the supervision of Dr. Amini in Mechanical Engineering at Persian Gulf University, Iran in 2018. His main research interests are heat transfer enhancement and fluid structure interaction.

Yasser Amini received his BSc, MSc, and PhD degrees in Mechanical Engineering from Shiraz University, Iran in 2006, 2009, and 2014, respectively. He is currently an Assistant Professor at the Department of Mechanical Engineering, Persian Gulf University, Iran. His main research interests include mesh-less methods, fluid structure interaction, heat transfer enhancement, transport in porous media, and piezoelectric energy harvesting.

Ehsan Izadpanah is an Associate Professor of Mechanical Engineering at Persian Gulf University, Iran. He received his MSc and PhD from Yazd University, Iran in 2006 and 2012, respectively. His research and teaching interests lie in the fields of heat transfer, thermal transport phenomenon, compact high-performance cooling technologies, and vortex induced vibration.